THE ASTROPHYSICAL JOURNAL, 381:526–533, 1991 November 10

DISCOVERY OF A LONG-TERM PERIODIC VARIATION IN LMC X-3

A. P. COWLEY,[1,2,3] P. C. SCHMIDTKE,[1,2,3] K. EBISAWA,[4] F. MAKINO,[4]
R. A. REMILLARD,[5] D. CRAMPTON,[1,2,6] J. B. HUTCHINGS,[1,2,6]
S. KITAMOTO,[7] AND A. TREVES[2,8]

Received 1991 February 22; accepted 1991 May 15

ABSTRACT

The highly variable X-ray luminosity of LMC X-3 is found to be strongly modulated with a period of ~ 198 (or possibly ~ 99) days. Observations from both *Ginga* and *HEAO 1* satellites show this periodic variation. For energies <13 keV, the X-ray intensity and hardness are positively correlated; for higher energies, there appears to be no correlation. Available optical photometry indicates the mean V brightness also varies by >1 mag with this same long-term period. The regularity of this "clock" in LMC X-3 suggests that it may be related to an accretion disk precession, similar to that seen in LMC X-4, Her X-1, SS 433, or possibly periodic variations in the mass transfer rate.

Subject headings: stars: individual (LMC X-3) — X-rays: binaries

1. INTRODUCTION

LMC X-3 has been known for many years as a highly variable X-ray source (e.g., Griffith & Seward 1977; Johnston, Bradt, & Doxsey 1979). It was shown by Cowley et al. (1983) to be a binary system which is likely to contain a black hole of $\sim 9\ M_{\odot}$ or more. Low-amplitude ellipsoidal variations of the B star companion support the hypothesis that LMC X-3 contains a massive, collapsed star (Khruzina & Cherepashchuk 1984; Kuiper, van Paradijs, & van der Klis 1988). Additionally, White & Marshall (1984; also see White 1989) pointed out that the ultrasoft X-ray spectrum of LMC X-3 made it similar to other black hole candidates such as Cyg X-1 and A0620−00, although it is not known if all ultrasoft binaries contain black holes.

In spite of the very large observed range in the X-ray flux, the variation does not occur on the time scale of the (1.7 day) orbital period, i.e., the variation is not due to an eclipse or partial occultation by a star or a prominence on the accretion disk (Cowley et al. 1983; White & Marshall 1984). Several groups have shown that the mean optical brightness varies by ~ 1 mag on a time scale much longer than the orbital period (Warren & Penfold 1975; van der Klis, Tjemkes, & van Paradijs 1983; van der Klis et al. 1985; van Paradijs et al. 1987). The long-term optical variation, with correction for the small (~ 0.2 mag) ellipsoidal orbital effects, has been shown to be correlated with the X-ray flux (van Paradijs et al. 1987), at least for one epoch.

The aim of our present study was to determine the character of the X-ray variability by studying the archival *HEAO 1* observations and by obtaining new data with the *Ginga* satellite. Since we also wanted to investigate how the X-ray and optical variations are correlated over a long time scale, optical photometry was obtained at CTIO. This paper presents an analysis of these data and concludes both the X-ray and optical flux vary periodically with a cycle time of ~ 198 (or possibly ~ 99) days.

2. X-RAY OBSERVATIONS AND LONG-TERM OPTICAL PHOTOMETRY

2.1. *HEAO 1 Data*

X-ray observations (1–13 keV) were made by *HEAO 1* with the Scanning Modulation Collimator (MC; Gursky et al. 1978). Since LMC X-3 lies near the ecliptic pole, it was almost always within 3° of the detector scan line for the 17 months of satellite operation. Detected counts in each scan of LMC X-3 ($\pm 2°$ in scan azimuth) were folded with the MC transmission function, and the signal was attributed to the source only if the phase was within a 4% selection window centered on the celestial position of LMC X-3. The analysis algorithm fits the MC data for two sources when a second X-ray detection is obtained. This ensures a proper modeling of the X-ray background when the scanning path produces some flux either from LMC X-1 or LMC X-4. The flux calibration was empirically guided by contemporaneous observations of the Crab Nebula.

Figure 1 shows a plot of the *HEAO 1* X-ray intensity (energy range 2–10 keV) versus Julian Date (in 1977–1978). The density of measurements shown in Figure 1 reflects the chosen integration time for that portion of the light curve. Depending on the intensity of LMC X-3 and the MC transmission efficiency (i.e., the scan elevation angle), we varied the sampling time between 3 hr and 5 days to balance both time resolution and statistical accuracy of the measurements. Even from a casual glance, one recognizes a modulation with ~ 100 day cycle. Four peaks are prominent.

Analysis of the *HEAO 1* data, using the method described by Stellingwerf (1978), shows two highly significant periods at 98.9 days and ~ 198 days, as illustrated in Figure 2. Both maxima in the periodogram are quite broad, and the one near $P \sim 198$ days is asymmetrical making it difficult to define the exact

[1] Visiting Astronomer, Cerro Tololo Inter-American Observatory, operated by the Association of Universities for Research in Astronomy, Inc., under contract with the National Science Foundation.

[2] Guest Observer on the *Ginga satellite*.

[3] Physics and Astronomy Department, Arizona State University, Tempe, AZ 85287.

[4] Institute of Space and Astronautical Science, 1-1 Yoshinodai 3-chome, Sagamiharashi, Kanagawa 229, Japan.

[5] Center for Space Research, Room 37-595, M.I.T., Cambridge, MA 02139.

[6] Dominion Astrophysical Observatory, 5071 West Saanich Road, Victoria, B.C., Canada, V8X 4M6.

[7] Physics Department, Faculty of Science, Osaka University, 1-1 Machikanoyamacho, Toyonaka-shi, Osaka 560, Japan.

[8] International School for Advanced Studies, 34014, Trieste, Italy.

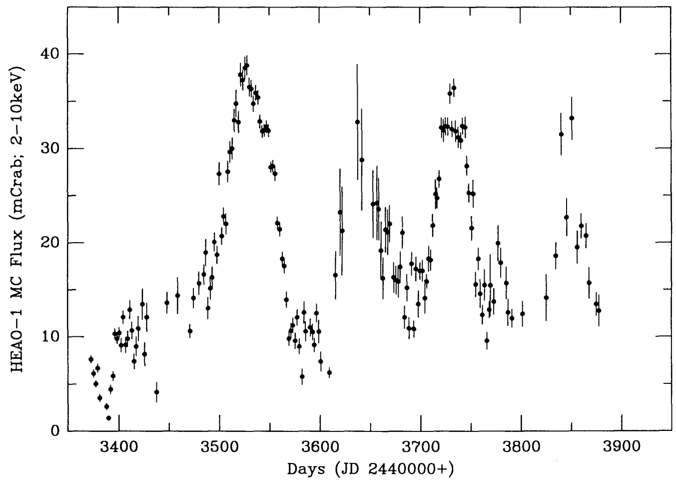

FIG. 1.—*HEAO 1* MC flux vs. Julian Date, showing the ~100/200 day periodicity.

value of the "best" period. If the period were 98.9 days, one would have expected a fifth intensity peak at the beginning of the data which is clearly not present. Alternately, the fundamental period could be ~198 days, with a strong intensity rise during each cycle followed by a less pronounced, secondary peak approximately 100 days later. The character of the data (e.g., the intensity range, shape, and width of both peaks, alternating high peaks, etc.) suggests the ~198 day period should be preferred. Examining all of the data, it is probable that during some cycles the secondary peak did not brighten as quickly as usual or was not present at all. This may be similar to the situation in Her X-1 where occasionally the 35 day cycle shows a delayed "turn on," generally thought to be due to obscuration of the X-ray source by additional material within the system (e.g., Crosa & Boynton 1980, and references therein). Figure 3*a* shows the *HEAO 1* data folded on the "best-fit" of the longer periods: 197.8 days.

2.2. *Ginga Data*

LMC X-3 was observed 35 times from 1987 March to 1990 March with the Large Area Counters (LAC) (Turner et al. 1989) on board the *Ginga* satellite (Makino & Astro-C Team 1987). The energy range of the LAC is 1.2–37 keV, with 48 channels in MPC1 and MPC2 modes and 12 in MPC3 mode (see Turner et al.). In addition to a dedicated series of pointed LMC X-3 observations, the LMC region was frequently monitored with the LAC in scanning and pointed modes to detect X-rays from SN 1987A. During some slewing operations to observe the supernova and occasionally while attitude maneuvering, the satellite field of view also crossed LMC X-3 by chance. Thus, in this study four different types of observations were used: (1) pointed, (2) scanning, (3) maneuvering, and (4) slewing.

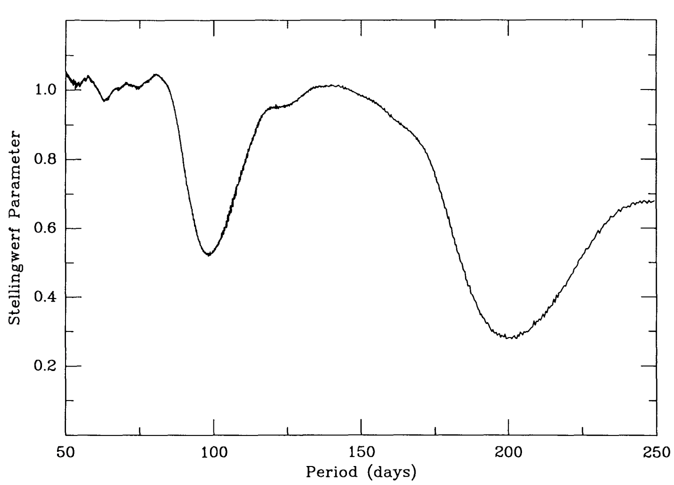

FIG. 2.—Significance vs. trial periods for the *HEAO 1* X-ray data

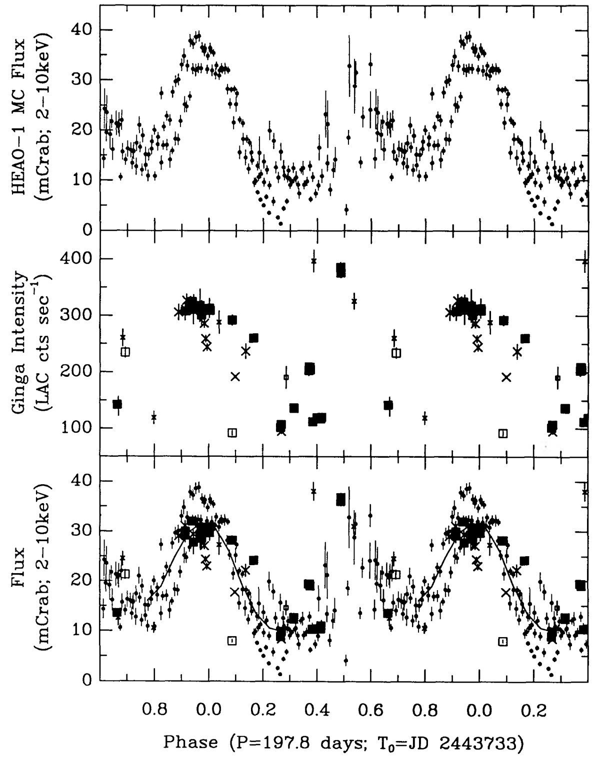

FIG. 3.—X-ray light curves on the 197.8 day period. Symbols for *Ginga* data are filled squares for pointed observations, large crosses for scans, open squares for maneuvering observations, and small crosses for slews. The *HEAO 1* data are shown by small filled circles. *Upper: HEAO 1* data; *middle: Ginga* data; *lower:* Combined *HEAO 1* and *Ginga* X-ray fluxes with a smooth curve that is a running average of observations through the primary intensity peak. T_0 = JD 2,443,733, which was adopted after fitting a parabola to the *HEAO 1* peak centered on that data.

For pointed and long-duration maneuver observations, the background was subtracted using the method described by Hayashida et al. (1989). For scans, the source intensity was determined by fitting the scan profile with an energy-dependent angular response function using three energy bands independently: 1.2–18.6 keV, 1.2–4.8 keV, and 4.8–9.3 keV (see Turner et al. 1989). The energy range above 9.3 keV could not be fitted because of poor statistics. During quick slews, with typical exposure times of only ~8 s, the source intensity was determined in the same way as for scans, but with less precision. A total of 45 data points was obtained, although if observations taken less than half a day apart are combined, the total is only 35. Details about the various *Ginga* observations are given in Table 1. Intensity errors are due to statistical fluctuations, uncertainty of the aspect of the spacecraft and estimation of the background.

Since there are considerably fewer data points from *Ginga*

TABLE 1

Ginga Data for LMC X-3

JD_{Mid} 2,400,000+	Net Exposure (s)	Type	Mode	Intensity 1.2–18.6 keV (LAC counts s^{-1})	Hardness: 4.7–9.3 keV/1.2–4.7 keV	Hardness: 9.3–18.6 keV/4.7–9.3 keV
6875.894.........	252	Scan	MPC1	306. ± 14.	0.28 ± 0.01	...
6880.877.........	128	Scan	MPC1	311. ± 10.	0.30 ± 0.01	0.03 ± 0.02
6881.671.........	116	Scan	MPC1	327. ± 11.	0.30 ± 0.01	...
6886.669.........	1076	Point	MPC1	311. ± 26.	0.278 ± 0.003	0.019 ± 0.007
6886.682.........	308	Scan	MPC1	308. ± 8.	0.31 ± 0.01	0.03 ± 0.02
6894.619.........	128	Scan		286. ± 7.	0.26 ± 0.01	0.05 ± 0.02
6895.615.........	128	Scan	MPC1	259. ± 6.	0.29 ± 0.01	0.04 ± 0.02
6896.519.........	248	Scan	MPC1	244. ± 6.	0.26 ± 0.01	0.04 ± 0.02
6917.042.........	224	Scan	MPC1	192. ± 2.	0.23 ± 0.01	0.03 ± 0.02
6924.885.........	120	Scan	MPC1	237. ± 13.	0.25 ± 0.02	0.11 ± 0.04
7103.153.........	8	Slew	MPC1	288. ± 20.	0.32 ± 0.04	0.13 ± 0.09
7168.767.........	2464	Point	MPC1	203. ± 9.	0.254 ± 0.002	0.085 ± 0.004
7168.979.........	7292	Point	MPC3	209. ± 2.	0.253 ± 0.001	0.092 ± 0.003
7169.469.........	29044	Point	MPC1	208.6 ± 0.9	0.251 ± 0.001	0.081 ± 0.003
7169.858.........	2382	Point	MPC3	204.3 ± 0.9	0.246 ± 0.001	0.076 ± 0.004
7227.744.........	8	Slew	MPC2	139. ± 17.	0.37 ± 0.09	0.17 ± 0.15
7230.895.........	8	Slew	MPC1	260. ± 15.	0.32 ± 0.04	0.13 ± 0.08
7232.610.........	1056	Maneuver	MPC1	234. ± 9.	0.252 ± 0.002	0.027 ± 0.006
7350.049.........	64	Maneuver	MPC1	191. ± 19.	0.21 ± 0.04	0.28 ± 0.15
7451.149.........	8	Slew	MPC1	119. ± 11.	0.26 ± 0.07	...
7508.423.........	3008	Maneuver	MPC1	92. ± 4.	0.173 ± 0.003	0.069 ± 0.015
7567.861.........	8	Slew	MPC1	397. ± 19.	0.37 ± 0.03	0.02 ± 0.05
7742.288.........	704	Scan	MPC1	95. ± 4.	0.24 ± 0.01	...
7785.442.........	4012	Point	MPC1	386. ± 9.	0.315 ± 0.001	0.053 ± 0.002
7785.556.........	5656	Point	MPC2	376. ± 8.	0.315 ± 0.001	0.049 ± 0.002
7795.166.........	4	Slew	MPC1	326. ± 14.	0.27 ± 0.03	0.07 ± 0.05
7820.157.........	3712	Point	MPC1	142. ± 3.	0.208 ± 0.002	0.006 ± 0.006
7869.593.........	569	Point	MPC3	308. ± 16.	0.290 ± 0.002	0.046 ± 0.004
7869.709.........	2192	Point	MPC1	308. ± 10.	0.291 ± 0.001	0.037 ± 0.002
7874.707.........	960	Point	MPC1	325. ± 7.	0.296 ± 0.002	0.043 ± 0.002
7880.413.........	704	Point	MPC1	318. ± 29.	0.290 ± 0.003	0.029 ± 0.007
7881.524.........	800	Point	MPC1	312. ± 15.	0.299 ± 0.002	0.039 ± 0.003
7881.573.........	862	Point	MPC3	301. ± 18.	0.294 ± 0.004	0.056 ± 0.006
7887.324.........	952	Point	MPC3	313. ± 17.	0.295 ± 0.003	0.050 ± 0.005
7887.877.........	7056	Point	MPC1	309. ± 4.	0.296 ± 0.001	0.040 ± 0.002
7904.098.........	5508	Point	MPC1	292. ± 9.	0.288 ± 0.001	0.041 ± 0.002
7919.611.........	1012	Point	MPC1	260. ± 7.	0.275 ± 0.002	0.055 ± 0.003
7939.368.........	1168	Point	MPC3	102. ± 3.	0.176 ± 0.004	0.051 ± 0.017
7939.932.........	8576	Point	MPC1	107. ± 3.	0.189 ± 0.002	0.048 ± 0.008
7949.049.........	2480	Point	MPC2	137. ± 3.	0.218 ± 0.003	0.076 ± 0.009
7949.160.........	2420	Point	MPC1	136. ± 3.	0.215 ± 0.002	0.055 ± 0.006
7962.783.........	2348	Point	MPC1	112.1 ± 1.5	0.186 ± 0.002	0.039 ± 0.008
7965.968.........	2790	Point	MPC1	119. ± 5.	0.179 ± 0.004	0.023 ± 0.016
7968.728.........	4544	Point	MPC3	117.4 ± 1.9	0.183 ± 0.002	0.018 ± 0.010
7969.397.........	14316	Point	MPC1	120.1 ± 1.6	0.191 ± 0.002	0.036 ± 0.007

than from *HEAO 1* and they are spread over 3 years, periodicities in these data are not at all obvious on visual inspection nor as straightforward to define. Figure 4 shows the *Ginga* intensity versus Julian Date (as given in Table 1). A period analysis was carried out using all the *Ginga* data. There is a maximum in the periodogram at ~111 days, and a less significant one at ~100 days. The 111 day period differs by ~10% from the primary period found in the *HEAO 1* data. However, for the majority of cycles there are only one or two observations, and therefore the period analysis is enormously sensitive to small changes in the observed intensity. For example, if the last four observations (obtained in 1990 March) are excluded, the most significant period drops to ~100 days. These observations are lower than would be expected, and they occur near phase ~0.4 in the 198.8 day ephemeris, suggesting another instance where the secondary peak was delayed. Optical photometry taken in 1990 April suggests the source eventually did brighten in this cycle. Further experimentation with the data also shows that small changes in the extracted intensity (which depends on the value of the background and the model) can significantly alter the derived period. This can be partially understood by looking at the folded intensity curve for the *HEAO 1* data (Fig. 3*a*) which shows that at any given phase, there is a large scatter in the observed intensity. However, the period analysis fits each observation to a smooth, average curve. Thus, with only one or two data points during each cycle, the period is very poorly defined. Therefore, instead of using a period derived independently from *Ginga* data, we

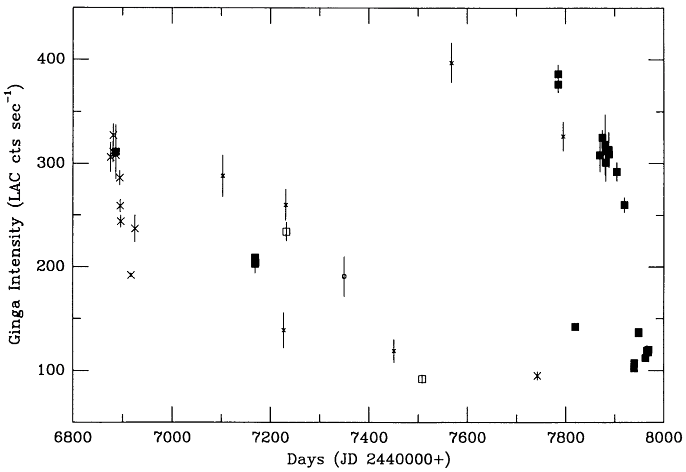

FIG. 4.—*Ginga* X-ray intensity as a function of Julian Date (1987–1990), using the same symbols as in Fig. 3.

examine how well it fits the *HEAO 1* period. Figure 3*b* shows *Ginga* intensities folded on the 197.8 day period.

2.3. *Other X-Ray Data*

Sunyaev et al. (1990) describe a limited number of observations which were made in 1988–1989 with the TTM telescope on board the Russian KVANT module. Although the data for LMC X-3 are not tabulated, their Figure 4 shows a plot of the X-ray counts, in the energy range 2–27 keV, as a function of Julian Date. The low intensity observed near JD 2,447,500 is in agreement with a low point in the *Ginga* data, and similarly their high-intensity point near JD 2,447,580 is matched by a very bright *Ginga* observation about a week earlier. The remaining TTM dates do not correspond to times of other known X-ray observations.

Seven observations of LMC X-3 were obtained with *EXOSAT*, primarily in 1984 (Treves et al. 1988). The data do not include the primary maximum, and they cover only a short range of phase (0.50–0.84) with an insufficient intensity range to constrain the long-term period. The most that can be said is that the *EXOSAT* data are not in conflict with the phasing and periodicity discussed here.

2.4. *Combined HEAO 1 and Ginga Data*

In order to search for the best overall period, the data were merged by converting the observed intensities to 2–10 keV flux, using mCrab units. The conversion of *Ginga* data makes explicit use of the energy spectrum while *HEAO 1* data require an assumed spectral shape. Period analysis, using the method described by Horne & Baliunas (1986), shows results similar to Figure 2 (*HEAO 1* alone), but with the broad envelopes resolved into a series of individual correlation peaks. For reasons described above (including alternating high/low peaks, evidence for missing peaks, etc.), we believe that the true cycle time is near 200 days. But since each cycle has two maxima, a best fit to the data appears to be obtained by doubling the ~ 100 day periods. Figure 5 shows the periodogram for periods near 100 days, with the most likely values marked. We interpret these as *half* the fundamental period and thus double these values to derive two possible long periods: 197.8 days or 202.7 days. These periods reflect a difference of one in the cycle count (on the ~ 100 day period) between *HEAO 1* and *Ginga* data sets. That is, the difference depends on which maximum in the observed *Ginga* light curve is fit the *HEAO 1* primary peak. A much superior fit of both X-ray and optical data is obtained using $P = 197.8$ days, and it also agrees with the best period found from the *HEAO 1* data alone. In Figure 3*c* all the X-ray data are folded on this period. Phase zero is adopted to be $T_0 =$ JD 2,443,733, which was found by fitting a parabola to the *HEAO 1* intensity peak centered on that date. Note that the secondary intensity maximum appears to be narrower and may not be centered between primary peaks.

2.5. *X-Ray Flux versus Hardness Ratio*

It was possible to obtain spectral information from most of the *Ginga* data. Figure 6 illustrates the spectral-hardness ratio versus X-ray intensity for two different energy ranges. The slew data are not included in the figure since the spectral information is very poorly determined for these short observations. It has been shown by Treves et al. (1990) that the X-ray energy spectrum of LMC X-3 can be expressed by two components: a soft, thermal component and a hard, power-law component. In the upper panel, the ratio of (4.7–9.3 keV)/(1.2–4.7 keV) is plotted against the (1.2–18.6 keV) intensity for the pointed, scan, and maneuver data. This soft component is believed to be emitted from the optically thick accretion disk around the black hole. There is a clear, positive correlation, suggesting the temperature of the disk rises with increasing intensity, although the intensity variations may be caused by geometric effects rather than intrinsic changes in the source itself (see § 3). The lower portion of Figure 6 shows the high-energy hardness ratio (9.3–18.6 keV)/(4.7–9.3 keV) plotted against (1.2–18.6 keV) intensity for the pointing and maneuvering data with good statistics. There is no correlation of these quantities. Thus, the hard component varies independently of the soft component. Similar uncorrelated behavior of the hard and soft components is found in LMC X-1 (Ebisawa, Mitsuda, & Inoue 1989), in the high state of GX 339-4 (Makishima et al. 1986), and in the X-ray nova GS 2000+25 (Tanaka 1989). All of these have been suggested as black hole candidates.

The hardness ratio was also examined for the *HEAO 1* data in two of the intensity peaks where the scan lines happened to pass directly over LMC X-3. The X-ray hardness ratio in both the (3–6 keV)/(1–3 keV) and (6–13 keV)/(3–6 keV) ranges are positively correlated with the X-ray flux. The brighter the

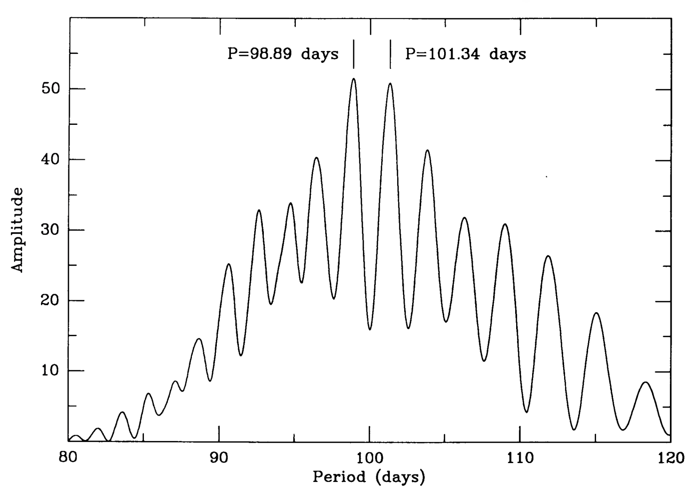

FIG. 5.—Significance vs. trial periods for the combined *HEAO 1* and *Ginga* data sets.

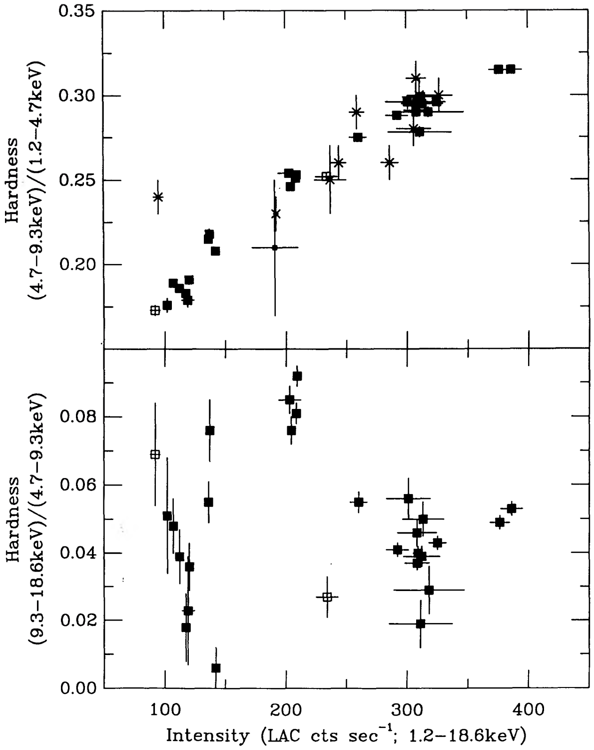

FIG. 6.—Intensity/hardness diagrams of LMC X-3 from *Ginga* data, using the same symbols as in Fig. 3. *Upper:* hardness ratio (4.7–9.3 keV)/(1.2–4.7 keV) vs. (1.2–18.6 keV) intensity; *lower:* hardness ratio (9.3–18.6 keV)/(4.7–9.3 keV) vs. (1.2–18.6 keV) intensity.

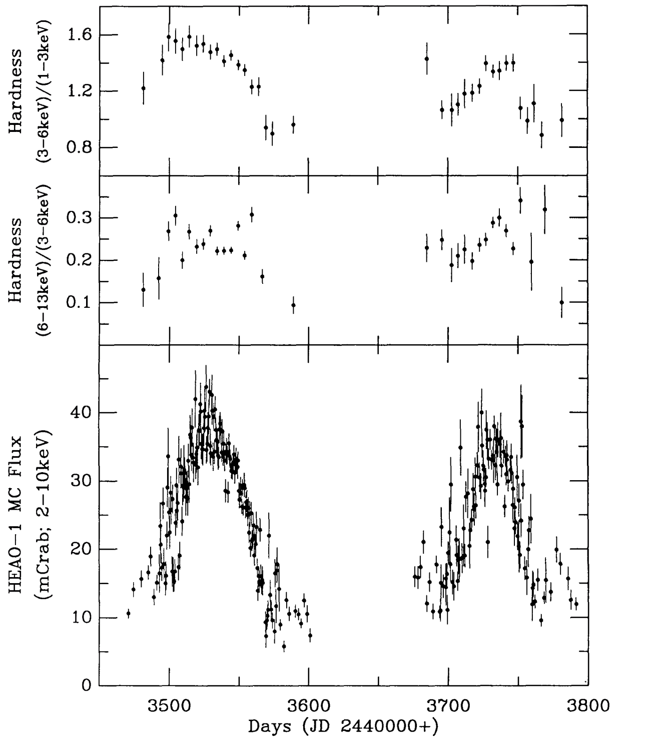

FIG. 7.—Two upper panels show hardness ratios in two different energy ranges: (3–6 keV)/(1–3 keV) and (6–13 keV)/(3–6 keV) vs. Julian Date for *HEAO 1* data. The lower panel shows the intensity curve for two of the primary peaks.

source, the greater the hardness ratio in both energy bins. This is shown in Figure 7 . Because of the limited amount of data available in the secondary peaks, it was not possible to analyze their intensity/hardness behavior. In principle, comparing the spectral information in successive strong-weak peaks might be a way of distinguishing between the ~198 day and ~99 day periods.

2.6. *Optical Photometry and Correlation with the X-Ray Light Curve*

Optical *BVR* photometry of LMC X-3 was obtained at CTIO in 1985 November, 1988 December, 1989 November/December, and 1990 April with CCD detectors on the 0.9 m and 1.5 m telescopes. The frames were reduced using DAOPHOT (Stetson 1987) and calibrated with similar observations of Landolt (1983, 1987) standard stars, following the guidelines of Schmidtke (1988). Figure 8 shows the *V* light curves for these observing runs to illustrate changes in the mean light level on a long time scale. The 1989 data, spanning nine nights, show a smooth ellipsoidal variation (~0.2 mag range) with little intrinsic scatter. This implies the mean light level was relatively constant during the observing run. Data from the other observing runs are consistent with the shape of the 1989 data and differ only in the mean light level.

We have also examined the variation of $(B-V)$ color. Figure 9 plots $(B-V)$ as a function of the 1.7 day orbital phase at various epochs using the CTIO photometry. During a single observing run (i.e., at a given mean light level), there is little or no evidence for a color change during the orbital cycle. However, the color of the system changes dramatically with the average system magnitude. Figure 10 shows $(B-V)$ as a

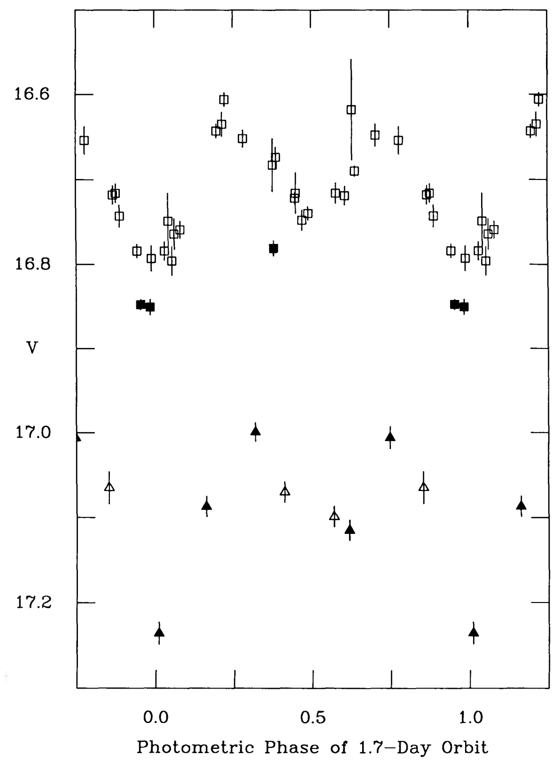

FIG. 8.—CTIO *V* light curves, plotted on the 1.7 day orbital period, using the ephemeris of van der Klis et al. (1985). Data from individual observing runs are shown by different symbols: open triangles (1985 November), filled triangles (1988 November/December), open squares (1989 December), and filled squares (1990 April). Note the change in mean light level between observing runs.

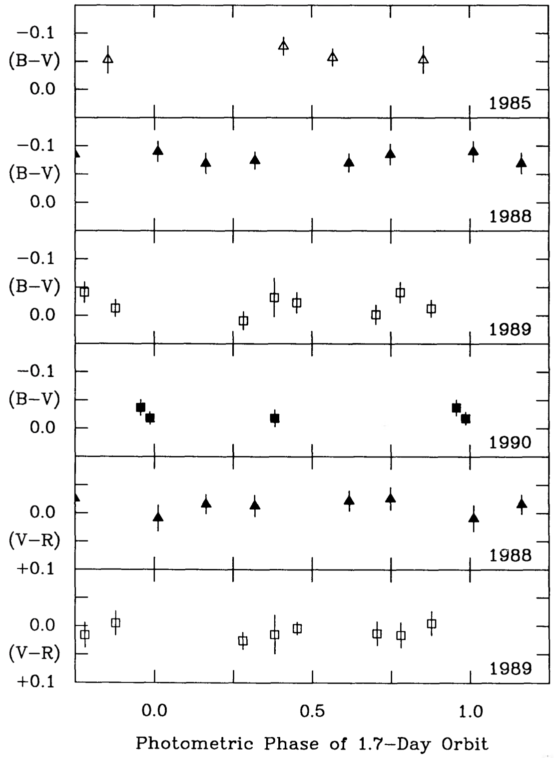

FIG. 9.—$(B-V)$ color as a function of the 1.7 day orbital phase at different epochs, using symbols from Fig. 8. Also shown in the $(V-R)$ color for the 1988 and 1989 observations. For a given epoch there is no orbital color change, within observational errors. However, the value of mean $(B-V)$ depends on the brightness of the system, as shown in Fig. 10.

function of V magnitude (after ellipsoidal variations have been removed, as described below) for all of the published and CTIO data. The plot shows a strong trend toward redder colors as the system brightens. Only the Warren & Penfold

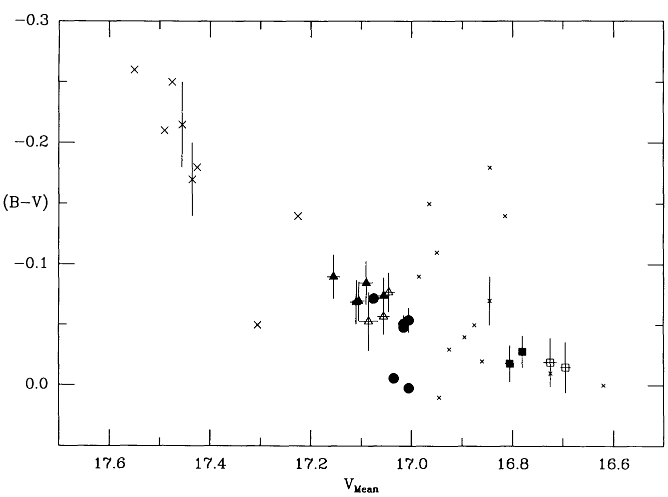

FIG. 10.—$(B-V)$ as a function of mean V magnitude (i.e., the average system magnitude, after ellipsoidal variations have been removed, as described in the text). The 1985–1990 data from CTIO use the same symbols as Fig. 8. Additional points are shown by filled circles for van der Klis (1985) (data taken in 1983), large crosses for van der Klis (1983) (data taken in 1981), and small crosses for Warren & Penfold (1975) as tabulated by Cowley et al. (1983). The system becomes much bluer when it is faint, indicating that the cooler accretion disk contributes substantially to color and magnitude at maximum light.

(WP; 1975) data (as tabulated by Cowley et al. 1983) show extreme scatter in this plot (*small crosses*). Since their photometry has larger errors (1.0 m telescope) and introduces scatter, we have not included WP data in subsequent optical analysis. (Note that the WP photometry also contributes to the scatter in Fig. 5 of van Paradijs et al.) All of the other available photometry show that LMC X-3 is considerably bluer when it is faint: $(B-V) \sim -0.25$ when $V \sim 17.6$, while $(B-V) \sim 0$ at $V \sim 16.7$. This indicates, in agreement with the work of Treves et al. (1988), that in the optical band the disk appears redder than the B star (although below we show that the disk's color is not constant).

We have combined the published and new (CTIO) optical photometry of LMC X-3 to search for correlations with the X-ray data and to see if the mean light level (i.e., the average magnitude, corrected for the 1.7 day ellipsoidal variations) is modulated on the 198 day period. For each data set we derived a nightly mean magnitude by removing the ellipsoidal variation in a manner similar to that described by van Paradijs et al. (1987). An average ellipsoidal light curve was constructed with an amplitude of 0.15 mag. This was then compared to all available photometry for each night separately, matching the orbital phase and sliding the standard curve to best fit that night's data. The mean light level could then be read directly from the observations. This process also revealed that the amplitude of the ellipsoidal variations changes with mean light level. When the source is bright ($V \sim 16.8$), the amplitude of the 1.7 day variation is about 0.15 mag. However, when the source is faint ($V \sim 17.5$), the amplitude increases to ~ 0.25 mag. This change would be expected if a light source which is constant on the 1.7 day period (presumably the disk) were added to the B star's ellipsoidal variations.

In our comparison we examined both the individual data sets and all of the photometry, folded on the most likely X-ray period ($P = 197.8$ days). Some of the CTIO photometry (1988 November/December and 1989 December) was taken within a few days of *Ginga* X-ray observations. In 1988 December both the X-ray and optical luminosity were low. On JD 2,447,505, $V_{\rm mean} = 17.18$ and 3 days later the *Ginga* intensity was 92 LAC counts s^{-1}. In 1989 December the system was bright (on JD 2,427,862, $V_{\rm mean} = 16.80$) and the *Ginga* X-ray intensity was high (305 LAC counts s^{-1}). Similarly, van Paradijs et al. (1987) showed that the optical magnitude was positively correlated with the *EXOSAT* X-ray intensity. Treves et al. (1990) found LMC X-3 to be very faint ($V \sim 17.5$) in 1988 January when the average *Ginga* countrate was at an intermediate level (~ 205 LAC counts s^{-1}). Since, their magnitudes were derived from spectrophotometric data rather than direct photometry, there could be an uncertainty of a few tenths of a magnitude in the transformation. In spite of this, their V magnitude fits reasonably well on the long-term light curve. Simultaneous *IUE* observations at ~ 2500 Å are also indicative of a low state. Unfortunately, much of the published photometry (e.g., Warren & Penfold 1975; van der Klis et al. 1983, 1985) was not obtained during known X-ray observations.

In Figure 11 we plot the nightly mean V magnitudes on the 197.8 day period. The optical photometry shows a light curve similar to a double-peaked structure seen in the 198 day X-ray cycle. Note that the phasing of the optical curve appears to be shifted with respect to the X-ray variations, with the optical maximum occurring $\sim 0.1P$ earlier. The solid line in Figure 11 shows the mean X-ray curve superposed on the photometry, with arbitrary scaling. The optical and X-ray light curves

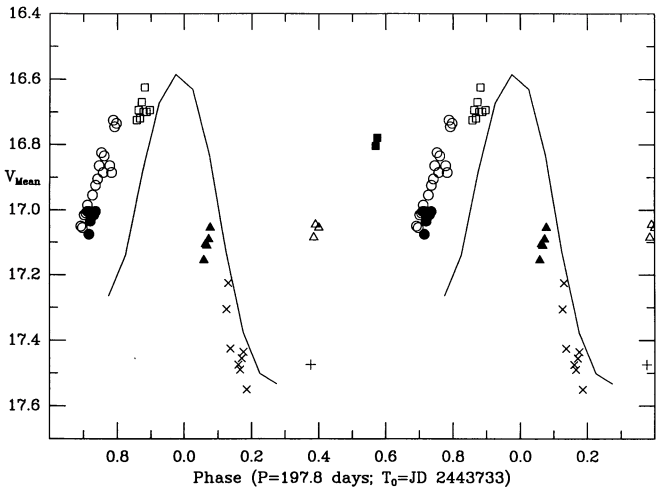

FIG. 11.—Mean V magnitude vs. phase on the 197.8 day period from CTIO observations and data in the literature. The symbols from Fig. 10 are used, with the addition of open circles for van Paradijs et al. (1987) and a plus sign for Treves et al. (1990). The solid curve represents the mean values from X-ray data shown in Fig. 3c, with arbitrary scaling chosen to give the data sets similar ranges on the plot. There appears to be a small ($\sim 0.1P$) phase shift of the optical data with respect to the X-ray curve.

appear to be similar in form but the optical maximum may have a broader primary peak. The secondary peak is too poorly defined in the optical data to compare with the X-ray curve.

The disk $(B-V)$ color as a function of disk brightness can be determined from the observed photometry of the system if we assume values for the magnitude and color of the B3 star. If the faintest points in Figure 10 primarily represent the B star (i.e., disk contribution very faint), we can adopt $V = 17.5$ and $(B-V) = -0.25$ for the intrinsic values of the star. This places the B star on the blue edge of the locus of points defining the LMC main sequence (cf. Hardy et al. 1984). An alternate way to assess the percentage contribution of the disk at minimum light would be to examine the dilution of absorptions lines in the spectra taken at appropriate phases. Cowley et al. (1983) showed (their Fig. 2) that the lines are considerably weakened (relative to a standard star) in spectra taken near maximum light, but we have no spectra at minimum. The calculated photometric parameters for the disk in LMC X-3 are shown in Figure 12, where the error bars represent only those errors that arise from the composite optical photometry and do not account for an uncertainty in the intrinsic stellar values. Changes in the later primarily yield a translation of the data points, possibly with a slight change in slope. As the disk brightens, or appears to brighten due to changing geometry (see § 3), the $(B-V)$ of the disk becomes bluer. Therefore, the correlation between optical color and magnitude, shown in Figure 10, is not caused by simple addition of light from the disk but represents the inclusion of a progressively bluer disk contribution.

3. DISCUSSION

There are several other massive X-ray binaries in which periods much longer than their orbital periods are present: 35 days in Her X-1 (Gerend & Boynton 1976, and references therein), 30 days in LMC X-4 (Lang et al. 1981; Heemskerk & van Paradijs 1989), and 164 days in SS 433 (Margon, Grandi, & Downes 1980, and references therein). It has been argued that each of these systems contains a thick, precessing accretion disk, and that the long-term variations are due to the changing aspect and/or obscuration by the disk. This may well be the cause of the long-term variation seen in LMC X-3.

The precessing accretion disk model relies on geometric factors associated with a structure that is known to change its size and shape. It provides a means of explaining that "sloppy clock" characteristic that the data portray. Treves et al. (1990) clearly showed that at least two X-ray spectral components are present, although the soft X-ray component strongly dominates the light curves presented above. If this component is optically thin and the X-ray modulation is primarily caused by gradual obscuration of the source by the accretion disk, then the data impose rather extreme conditions on the structure of the disk. It is striking that the X-ray flux is softer at lower intensity, implying that absorption due to photoelectric ionization plays no appreciable role in the X-ray modulation. Therefore, either the inner, ionized disk is warped at angles exceeding $\pm 25°$, the complement of the "best-fit" inclination angle in this noneclipsing binary (see Kuiper et al. 1988), or the profile of the outer disk (not fully ionized) is surprisingly sharp, has a thickness of at least 0.2 in phase (see Fig. 3), and yet provides no line of sight that intercepts column densities in the range $\log N_H = 22$–24 cm^{-2}, where absorption effects would be evident (Morrison & McCammon 1983). In contrast, LMC X-4 and Her X-1 are both observed at high inclination angles, exhibiting binary eclipses (Lang et al. 1981; Tananbaum et al. 1972), and Her X-1 shows evidence of photoelectric absorption during precession-ingress and aperiodic intensity dips (Becker et al. 1977; Vrtilek & Halpern 1985).

Perhaps a more plausible precession scenario for LMC X-3 can be found with optically thick models for the soft X-ray component, where the X-ray modulation may largely depend on the orientation of the emitting region itself as the accretion disk precesses. In the disk-blackbody model of Treves et al. (1990), the optical depth perpendicular to the disk is large, and the observed flux may scale with the cosine of the disk-viewing angle (with additional modifications dependent on the flatness of the inner disk and likely complications related to dynamical effects near the black hole's Schwarzschild radius). The disk may be geometrically thinner compared with the case related to an obscuration-based explanation, and any absorption

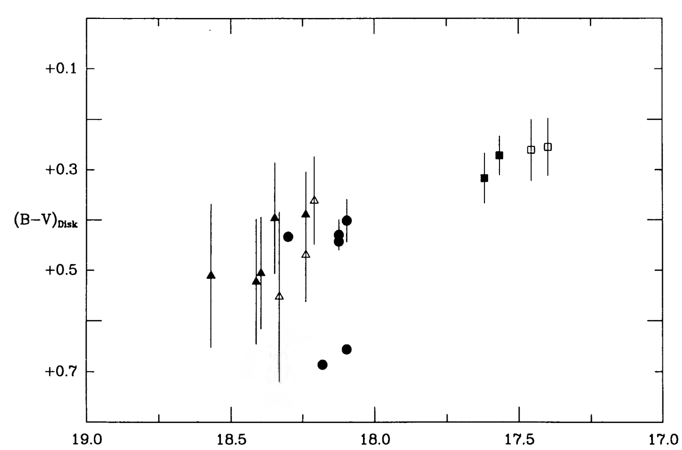

FIG. 12.—$(B-V)$ vs. V for the disk, found by subtracting the contribution of a $V = 17.5$, $(B-V) = -0.25$ star from the composite photometry. The apparent color of the disk becomes bluer as the disk brightens.

effects would occur closer to the intensity minima where they are statistically more difficult to measure. There remains a requirement for significant thickness changes in the disk with time in order to explain the variability in the secondary maxima. It may be necessary to invoke an additional soft component that is spatially extended, such as an accretion disk corona, in order to explain the fact that X-ray minima are usually $\sim 20\%$ of the maxima.

An alternate explanation for the long-term periodic variation is that the temperature change, manifested in both X-rays and optical light, is mainly due to the change of the mass accretion rate. If each radial part of the disk emits as a blackbody, the local luminosity and temperature at a given radius is proportional to $\dot{M}$ and $\dot{M}^{1/4}$, respectively. Detailed X-ray spectral study has shown that the spectral change of the soft X-ray component can be successfully explained in this manner. A quantitative discussion of the X-ray spectral variation is presented in a separate paper (Ebisawa et al. 1991).

Note that the two mechanisms, precession and variation in mass transfer, discussed above do not exclude each other. It may be possible that the disk precession modulates the mass accretion rate according to the change of the relative disk configuration as " seen " by the mass-donating companion star.

Our LMC X-3 data, when broken into subsamples, suggest that the exact value of long period may vary slightly from epoch to epoch. However, this is not unexpected as the precession period in both SS 433 (Margon & Anderson 1989) and Her X-1 (Boynton, Crosa, & Deeter 1980) exhibit variations of about 5%. Iping & Petterson (1990) have shown that substantial deviations ($\sim 10\%$ or more) from precessional periodicity can occur when variable X-ray emission on the warp-structure of the disk is taken into account.

It has been noted (e.g., Petterson 1985) that the ratio of precession/orbital periods is similar in X-ray binaries which show both periods: 22 for LMC X-4, 20 for Her X-1, and 13 for SS 433. However, for LMC X-3 the long period is 116 times greater than the orbital period. Even if the fundamental long period were ~ 99 days, the ratio would still be much larger (58 times) than for the other systems.

In summary, both the X-ray and optical luminosity of the black hole binary LMC X-3 show a pronounced, periodic variation on a ~ 198 day cycle, with alternating strong and weak intensity peaks. It is suggested that this variation may arise from precession of the accretion disk, as has been found for several other well-studied X-ray binaries, or from variations in the mass accretion rate, or even a combination of the two.

We acknowledge the contribution of all members of the *Ginga* team in providing the LMC X-3 observations used in this paper. A. P. C and P. C. S. particularly thank the scientists and staff at ISAS and CTIO who were extremely helpful during our visits to their institutions. A. P. C. gratefully acknowledges support from NASA (NAG 8-756) and NSF (AST 8815450) grants. R. A. R. acknowledges NASA Grants NAG 8-673 and NAG 8-493.

REFERENCES

Becker, R. H., et al. 1977, ApJ, 214, 879
Boynton, P. E., Crosa, L. M., & Deeter, J. E. 1980, ApJ, 237, 169
Cowley, A. P., Crampton, D., Hutchings, J. B., Remillard, R., & Penfold, J. E. 1983, ApJ, 272, 118
Crosa, L., & Boynton, P. E. 1980, ApJ, 235, 999
Ebisawa, K., Makino, F., Mitsuda, K., Belloni, T., Cowley, A. P., Schmidtke, P. C., & Treves, A. 1991, in 23d Yamada Conference on Frontiers of X-ray Astronomy, ed. K. Koyama, in press
Ebisawa, K., Mitsuda, K., & Inoue, H. 1989, PASJ, 41, 519
Gerend, D., & Boynton, P. E. 1976, ApJ, 209, 562
Griffiths, R. E., & Seward, F. D. 1977, MNRAS, 180, 75P
Gursky, H., et al. 1978, ApJ, 223, 973
Hardy, E., Buonanno, R., Corsi, C. E., Janes, K. A., & Schommer, R. A. 1984, ApJ, 278, 592
Hayashida, K., et al. 1989, PASJ, 41, 373
Heemskerk, M. H., & van Paradijs, J. A. 1989, A&A, 223, 154
Horne, J. H., & Baliunas, S. L. 1986, ApJ, 302 757
Iping, R. C., & Petterson, J. A. 1990, A&A, 239, 221
Johnston, M. D., Bradt, H. V., & Doxsey, R. E. 1979, ApJ, 233, 514
Khruzina, T. S., & Cherepashchuk, A. M. 1984, Soviet Astr., 28, 173
Kuiper, L., van Paradijs, J., & van der Klis, M. 1988, A&A, 203, 79
Landolt, A. U. 1983, AI, 88, 439
———. 1987, private communication
Lang, F. L., et al. 1981, ApJ, 246, L21
Makino, F., & Astro-C Team. 1987, Ap. Letters Comm., 25, 223
Makishima, K., Maejima, Y., Mitsuda, K., Bradt, H. V., Remillard, R. A., Tuohy, I. R., Hoshi, R., & Nakagawa, M. 1986, ApJ, 308, 635
Margon, B. H., & Anderson, S. F. 1989, ApJ, 347, 448
Margon, B., Grandi, S. A., & Downes, R. A. 1980, ApJ, 241, 306
Morrison, R., & McCammon, D. 1983, ApJ, 270, 119
Petterson, J. A. 1985, in Galactic and Extragalactic Compact X-Ray Sources, ed. Y. Tanaka & W. H. G. Lewin (Tokyo: Inst. of Space and Astronautical Science), 183
Schmidtke, P. C. 1988, AJ, 95, 1528
Stellingwerf, R. F. 1978, ApJ, 224, 953
Stetson, P. B. 1987, PASP, 99, 191
Sunyaev, R., et al. 1990, Soviet Astr.—Letters, 16, 55
Tanaka, Y. 1989, in Proc. 23rd ESLAB Symp., ed. J. Hunt & B. Battrick (ESA SP-296) (Paris: ESA), 1, 3
Tananbaum, H., Gursky, H., Kellogg, E. M., Levinson, R., Schreier, E., & Giacconi, R. 1972, ApJ, 174, L143
Treves, A., Belloni, T., Bouchet, P., Chiappetti, L., Falomo, R., Maraschi, L., & Tanzi, E. G. 1988, ApJ, 335, 142
Treves, A., et al., 1990, ApJ, 364, 266
Turner, M. J. L., et al. 1989, PASJ, 41, 345
van der Klis, M., Clausen, J. V., Jensen, K., Tjemkes, S., & van Paradijs, J. 1985, A&A, 151, 322
van der Klis, M., Tjemkes, S., & van Paradijs, J. 1983, A&A, 126, 265
van Paradijs, J., et al. 1987, A&A, 184, 201
Vrtilek, S. D., & Halpern, J. P. 1985, ApJ, 296, 606
Warren, P. R., & Penfold, J. E. 1975, MNRAS, 172, 41P
White, N. E. 1989, Astr. Ap. Rev., 1, 85
White, N. E., & Marshall, F. E. 1984, ApJ, 281, 354